Journal of Environmental Management 207 (2018) 70–79

Contents lists available at ScienceDirect

Journal of Environmental Management

journal homepage: www.elsevier.com/locate/jenvman

Research article

Combined strategy for removal of Reactive Black 5 by biomass sorption on *Macrocystis pyrifera* and zerovalent iron nanoparticles

Fabiana E. García [a], Josefina Plaza-Cazón [b], V. Nahuel Montesinos [c], Edgardo R. Donati [b], Marta I. Litter [c, d, *]

[a] Gerencia Química, Comisión Nacional de Energía Atómica, Av. Gral. Paz 1499, 1650, San Martín, Prov. de Buenos Aires, Argentina
[b] CINDEFI (CCT-La Plata, CONICET, UNLP), 50 y 115, La Plata, Argentina
[c] Gerencia Química, Comisión Nacional de Energía Atómica, CONICET, Av. Gral. Paz 1499, 1650, San Martín, Prov. de Buenos Aires, Argentina
[d] Instituto de Investigación e Ingeniería Ambiental, Universidad Nacional de Gral. San Martín, Campus Miguelete, Av. 25 de Mayo y Francia, 1650, San Martín, Prov. de Buenos Aires, Argentina

ARTICLE INFO

Article history:
Received 15 August 2017
Received in revised form
31 October 2017
Accepted 2 November 2017
Available online 12 December 2017

Keywords:
Reactive Black 5
RB5
Zerovalent iron nanoparticles
Macrocystis pyrifera

ABSTRACT

Reactive Black 5, RB5, has been used as a model azo dye to evaluate the removal efficiency of sorption on *Macrocystis pyrifera* biomass (*Mpyr*) and commercial zerovalent iron nanoparticles (nZVI) in individual and combined treatments. The best conditions for the treatment with the isolated materials were first determined, and then, in series and combined treatments were performed under these conditions, achieving removal efficiencies higher than 80% of the initial dye concentration. Strengths and weaknesses of all removal strategies (individual, in series and combined) are analyzed regarding the application on real effluents. *Mpyr* efficiently adsorbed RB5, but also increased the total organic content by partial dissolution of components of the algal biomass. Removal experiments with commercial nZVI were also efficient but liberated Fe to the solution, and sulfanilic acid was observed after the treatment as a product of RB5 degradation. In contrast, after the *Mpyr* treatment, no sulfanilic acid was detected, suggesting that sulfanilic acid is efficiently adsorbed by the biomass. The best condition was the integrated use of *Mpyr* and nZVI, with a remarkable removal efficiency (69–80%) obtained after only 1 h of treatment. Finally, nZVI were successfully immobilized in *Mpyr*, and the hybrid material was used to remove RB5 in continuous flow experiments at pH 3, obtaining a removal capacity of 39.9 mg RB5 g^{-1} after a total processed volume of 630 mL of $[RB5]_0 = 100$ mg L^{-1}.

1. Introduction

Azo dyes, which account for about 50% of all reactive dyes, are persistent compounds in the environment, known to be toxic, carcinogenic and mutagenic or teratogenic (Chatterjee et al., 2010; El-Zawahry et al., 2016; Iscen et al., 2007). Reactive Black 5 (RB5) is an azo dye widely used for textiles (Huang et al., 2016), and large amounts of this dye are discharged in watercourses of developing countries, impacting on ecosystems and humans (El-Zawahry et al., 2016; Huang et al., 2016; Iscen et al., 2007). The chemical structure of RB5 is illustrated in Fig. 1.

Processes traditionally used to remove dyes, such as adsorption, membrane filtration, ion exchange, chemical oxidation, electrochemical degradation, ozonation, and biological degradation, are in many cases ineffective, expensive or time consuming (Huang et al., 2016; Iscen et al., 2007). Due to the complex composition of real industrial effluents, no single process can be adequately applied, and the use of combined strategies must be envisaged (Crini, 2006).

From all methods, adsorption has been found to be superior in terms of flexibility and simplicity of design, initial cost, and easiness of operation, not producing harmful byproducts (Huang et al., 2016). In particular, biosorption can be a convenient low-cost technology for removal of dyes, where a variety of pretreated and immobilized forms of organisms (biomass) carry a wide range of binding sites for dyes (Iscen et al., 2007). Biosorption proceeds through a combination of active and passive transport mechanisms including ion-exchange and complexation, and functional groups such as amino, carboxylate, phosphate and hydroxyl are

* Corresponding author. Gerencia Química, Comisión Nacional de Energía Atómica, CONICET, Av. Gral. Paz 1499, 1650, San Martín, Prov. de Buenos Aires, Argentina.
E-mail addresses: marta.litter@gmail.com, litter@cnea.gov.ar (M.I. Litter).

https://doi.org/10.1016/j.jenvman.2017.11.002
0301-4797/

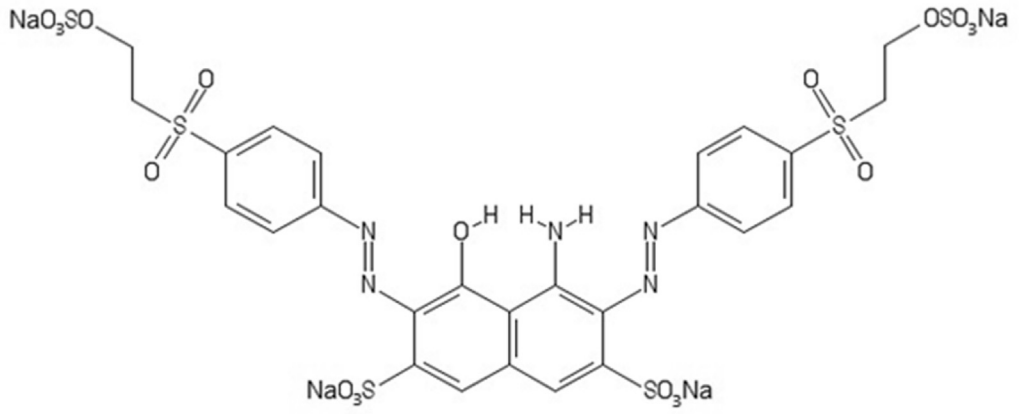

Fig. 1. Chemical structure of RB5.

responsible for the sequestration of hazardous materials (Iscen et al., 2007). A few bioadsorbents have been tested for RB5 removal, such as a biopolymer composite of cellulose extracted from water hyacinth *Eichhornia crassipes*, functionalized by chitosan and TiO_2 nanoparticles (El-Zawahry et al., 2016), and dried *Penicillium restrictum* biomass (Iscen et al., 2007).

Marine algae or seaweeds are abundant and available, and their capacity as biosorbents for heavy metals and dyes has been reported (e.g., Fakhry Eman, 2013; Low et al., 1994; Rubín et al., 2010; Yagub et al., 2014). In particular, the brown seaweed *Laminaria* sp. has been indicated as an excellent biosorbent of RB5 (Vijayaraghavan and Yun, 2008). *Macrocystis pyrifera*, belonging to Phaeophyceae (brown algae) lineage, is largely distributed in coastal regions of Mexico, USA, Peru, Chile, Argentina, South Africa, Australia, New Zealand and the Sub-Antarctic Islands (Miller et al., 2016). In Argentina, *Macrocystis pyrifera* can be found from Chubut to Tierra del Fuego (Boraso and Zaixo, 2012), and large amounts of this species are deposited on Bahía de Camarones beach (Chubut province). *Macrocystis pyrifera* has been studied as a low-cost adsorbent for Hg(II), Zn(II), Cd(II), Ni(II), Cr(III), and Cr(VI) removal with promising results (Plaza et al., 2011, 2012a,b; Plaza Cazón et al., 2013a,b; Plaza Cazón et al., 2014).

Zerovalent iron nanoparticles (nZVI) have been reported as powerful materials for removal of a wide variety of pollutants, including heavy metals, nitroaromatics, halogenated organics and dyes (Sun et al., 2016 and references therein). nZVI have usually a core of α-Fe and an outer shell formed by a complex mixture of iron oxy(hydroxides) (Montesinos et al., 2014). Thus, the combination of a moderate reducing power ($E^0 = -0.44$ V) from the core and a high surface area from the shell gives rise to a versatile material useful for adsorbing and/or reducing water pollutants. In this sense, azo dyes can be removed from water via reduction of the azo bond (Fan et al., 2009). Previous studies of RB5 treatment with micrometric or nanoscale zerovalent iron particles have been reported (Chatterjee et al., 2010; Chompuchan et al., 2009; Satapanajaru et al., 2011). However, the cleavage of the azo bonds by advanced methods leads to discoloration of the dye solution, generally with the generation of toxic amino aromatic products (Raman and Kanmani, 2016). Few studies proposed the degradation mechanism of dye molecules using nZVI recording intermediates or end products and TOC removal. Moreover, very limited studies are available in the integration of nZVI with other treatment techniques to degrade textile dyes, with the exception of that of Shang et al. (2017), who reported the removal of chromium (VI) from water with good efficiency using the integration of nZVI supported on herb-residue biochars.

In this paper, RB5 has been used as a model azo dye to evaluate the efficiency of sorption with *Macrocystis pyrifera* biomass (*MPyr*) and nZVI removal in individual and combined treatments.

2. Experimental

2.1. Materials and chemicals

RB5 was Vilmafix Black B-V. Iron nanoparticles (NANOFER 25, hereafter N25) were provided by NANO IRON, s.r.o. (Czech Republic) as a concentrated aqueous suspension ($[Fe_{total}] = 242$ g L^{-1}). The main physicochemical characteristics of N25 can be found in Appendix A, section S1, Supplementary data. H_2SO_4, NaOH, $CaCl_2$ and $FeCl_3 \cdot 6H_2O$ were Biopack; $(NH_4)_2Fe(SO_4)_2 \cdot 6H_2O$ (Mallinckrodt), H_3PO_4 (Anedra), CH_3OH (J.T. Baker) and sulfanilic acid (Sigma-Aldrich) were used. All reagents were of analytical quality or higher. 5 N H_2SO_4 or 4 M NaOH were used for pH adjustments. *Macrocystis pyrifera* was gathered in Bahía de Camarones. Algae biomass (*Mpyr*) was ground and sieved, and the 10–16 mesh (i.e., 1.18–2 mm) particle size was selected for the assays. Biomass was washed several times with distilled water and treated for 24 h with 0.2 M $CaCl_2$ at pH 5.0. Then, the biomass was dried in an oven at 50 °C for 48 h. In all experiments, Milli-Q water was used (resistivity = 18 MΩ cm).

2.2. RB5 biosorption experiments with Macrocystis pyrifera biomass (Mpyr)

In a typical experiment, 100 mL of an aqueous RB5 solution were put in an Erlenmeyer flask with the corresponding amount of *Mpyr*, and the flask was placed on an orbital shaker (Pro-Vicking) at 180 rpm in a controlled-temperature room at 25 °C for 600 min; 5 mL samples were periodically withdrawn to determine changes in the RB5 concentration. It was determined that 6 h of contact time (CT) was enough to reach the maximum changes (see section 3.1).

The influence of pH was studied in similar conditions of volume, agitation and temperature with 50 mg L^{-1} RB5 and 0.1 g of *Mpyr* at different initial pH values (1.0–4.0) adjusted with H_2SO_4. To study the effect of the biomass load, different amounts of *Mpyr* (0.1–4.0 g) were put in contact with the 50 mg L^{-1} RB5 solution. The effect of RB5 initial concentration was evaluated by mixing 0.6 g of *Mpyr* with RB5 solutions of different initial concentrations (40–400 mg L^{-1}) at pH 1 and 6 h CT.

The amount of adsorbed RB5 was calculated in all cases by the mass balance equation:

$$q = \frac{V([RB5]_0 - [RB5]_t)}{m} \quad (1)$$

where q is the solute uptake (mg g^{-1}), $[RB5]_0$ and $[RB5]_t$ are the concentrations of RB5 at time 0 and t (mg L^{-1}), respectively, V is the solution volume (L) and m is the biosorbent mass (g, dry weight basis).

The dye removal efficiency was calculated with the following equation:

$$\%R_{RB5} = \frac{([RB5]_0 - [RB5]_t) \times 100}{[RB5]_0} \quad (2)$$

2.3. Treatment of RB5 with N25

In a typical experiment, a given volume of N25 was taken from a vigorously agitated slurry using a vortex agitator orbital shaker (Decalab) and added to 30 mL of a 100 mg L^{-1} RB5 solution in an Erlenmeyer flask at a fixed pH adjusted with H_2SO_4 or NaOH. All experiments were carried out under continuous agitation at 215 rpm at room temperature using an orbital shaker (Vicking M-23). The effect of N25 loading (0.05–0.5 g L^{-1}) and pH (1.0–9.0) were tested. Samples were collected at regular times and centrifuged with an Eppendorf MiniSpin at 13,000 rpm for 5 min in a time span of 3 h to measure the remaining [RB5], total Fe concentration ($[Fe_{total}]$) and total organic carbon (TOC).

2.4. RB5 degradation combining Mpyr and N25

RB5 removal ($[RB5]_0$ = 100, 200 and 400 mg L^{-1}) was tested using three different experimental in series and combined treatment configurations: 1) *Mpyr* followed by N25 (*Mpyr*/N25); 2) N25 followed by *Mpyr* (N25/*Mpyr*), and 3) simultaneous use of *Mpyr* and N25 (*Mpyr* + N25). The best experimental conditions determined in individual experiments for RB5 removal using *Mpyr* and N25 were used, i.e., 6 g L^{-1} of *Mpyr* at pH 1 and 0.5 g L^{-1} of N25 at pH 3 (*vide infra*, sections 3.1 and 3.2). For configurations 1 and 2, RB5 removal with *Mpyr* was performed at pH 1, while the treatment with N25 was carried out at pH 3. In the case of simultaneous removal with *Mpyr* and N25, experiments were carried out at both pH 1 and 3. In all experiments, 3 mL samples were processed as described in the previous sections to measure [RB5], $[Fe_{total}]$ and TOC.

2.5. RB5 degradation in packed columns with N25 supported on Mpyr

N25 was supported on the surface of *Mpyr* by wet impregnation. Briefly, 4 mL of the N25 slurry were introduced in a sealed vial containing 0.2 g of *Mpyr* under N_2 atmosphere. The mixture was stirred for 24 h at room temperature and then water was removed by evaporation under a N_2 current (0.35 mL min^{-1}). After drying, the solid N25 supported on *Mpyr* (N25@*Mpyr*) was separated from the remaining iron not attached to the algae biomass using a 1 mm opening sieve (equivalent to No. 18 mesh sieve).

The solid was analyzed by SEM-EDS and XRD. SEM studies were carried out using an Environmental Scanning Electron Microscopy (ESEM) (Quanta 200 FEG, FEI, USA), equipped with an OXFORD Inca 350 Energy Dispersive X-ray microanalysis (EDS) system. XRD patterns were obtained using a Pan Analytical Empyrean X-ray diffractometer with PIXcel 3D detector, using Cu-Kα radiation, over a range in 2θ of 10–100° with step of 0.026° and 24 s by step.

RB5 removal ($[RB5]_0$ = 100 mg L^{-1}, pH 3) with N25@*Mpyr* was carried out in a glass column (5 cm length and 0.5 cm internal diameter) containing 0.6 g of the material packed in 3.6 cm length giving a column volume of 0.7 mL (calculated as $L \times \pi \times r^2$, where L is the column length and r is the radius of the column (0.25 cm)). The pore volume was 0.15 mL, calculated by the water mass excluded after filling N25@*Mpyr* into the column. The experiments were done at a continuous flow of 0.35 mL min^{-1}. Samples were periodically withdrawn to determine the evolution of [RB5], TOC and $[Fe_{total}]$.

2.6. Analytical methods

RB5 concentration in solution was measured by direct UV–Vis spectrophotometry at λ = 594 nm, using a UV/VIS HP8453A spectrophotometer. No other intermediates or products from RB5 absorb at that wavelength. pH determination was carried out using a METERLAB PHM290 pH-Stat Controller. TOC was measured with a TOC Shimadzu 5000 analyzer, in the NPOC (non-purgeable organic carbon) mode.

$[Fe_{total}]$ was measured by Total Reflection X-ray Fluorescence (TXRF) using Ga (100 mg L^{-1}) as internal standard. A S2 Picofox TXRF spectrometer was used.

For analysis of the RB5 degradation products after the in series treatments (*Mpyr*/N25 and N25/*Mpyr*), samples before and after each removal step were taken and analyzed by HPLC. For this purpose, 20 μL of each sample were injected at a flow rate of 1 mL min^{-1} in a Waters 1525 Binary HPLC Pump, equipped with a symmetric C18 column (4.6 × 150 mm Autosampler 717 Waters) and a Waters 2996 PAD detector, measuring at λ = 266 nm. A mixture of 90% acid phosphoric pH 2.1 and 10% methanol was used as the mobile phase.

3. Results and discussion

3.1. Treatment of RB5 with Mpyr in batch

Results of RB5 (50–400 mg L^{-1}) removal experiments with *Mpyr* (1–40 g L^{-1}) at pH 1 to 4 are shown in Fig. 2.

The major component of the algae biomass is alginic acid, a polymer composed of unbranched chains of 1,4-linked β-D-mannuronic acid and α-L-guluronic acids. Calcium-treated algae are more resistant to the leaching of some organic components from the biomass (which can be responsible for binding to the dye) (Matheickal and Qiming, 1999; Montesinos et al., 2014).

Fig. 2A shows a rapid increase of the removal efficiency ([RB5] = 50 mg L^{-1}, [*Mpyr*] = 6.0 g L^{-1}, pH 1) up to 120 min, followed by a slower increase up to 600 min. This increase on the biosorption capacity with the increasing CT was attributed to the availability of biosorption sites on the biomass surface (Iscen et al., 2007). About 92% (7.66 mg g^{-1}) of the initial dye was retained by *Mpyr* within 360 min (6 h) and, therefore, 6 h was fixed as the optimum CT. Fig. 2B shows that RB5 removal ([RB5] = 50 mg L^{-1}, [*Mpyr*] = 6.0 g L^{-1}, 6 h CT) decreased with pH, the maximum RB5 uptake (71.5%, 6 mg g^{-1}) being obtained at pH 1. This effect can be attributed to the higher protonation of the amine active site in *Mpyr* at this pH, provoking a strong electrostatic interaction with the very negative $-SO_3^-$ groups of the dye molecules even at pH 1 (Iscen et al., 2007) (the pK_a values of the sulfonate groups of the dye are estimated to be below −1 (Guthrie, 1978)). Fig. 2C shows that the removal efficiency ([RB5] = 50 mg L^{-1}, pH 1, 6 h CT) significantly increased with the sorbent biomass dosage, with the maximum dye uptake (96%, 8 mg g^{-1}) being achieved using 6 g L^{-1} of *Mpyr*. This maximum can be explained because there is an excess of the biosorption sites with the increase of the adsorbent load, which cannot be occupied by the adsorbate (Iscen et al., 2007). Fig. 2D shows that

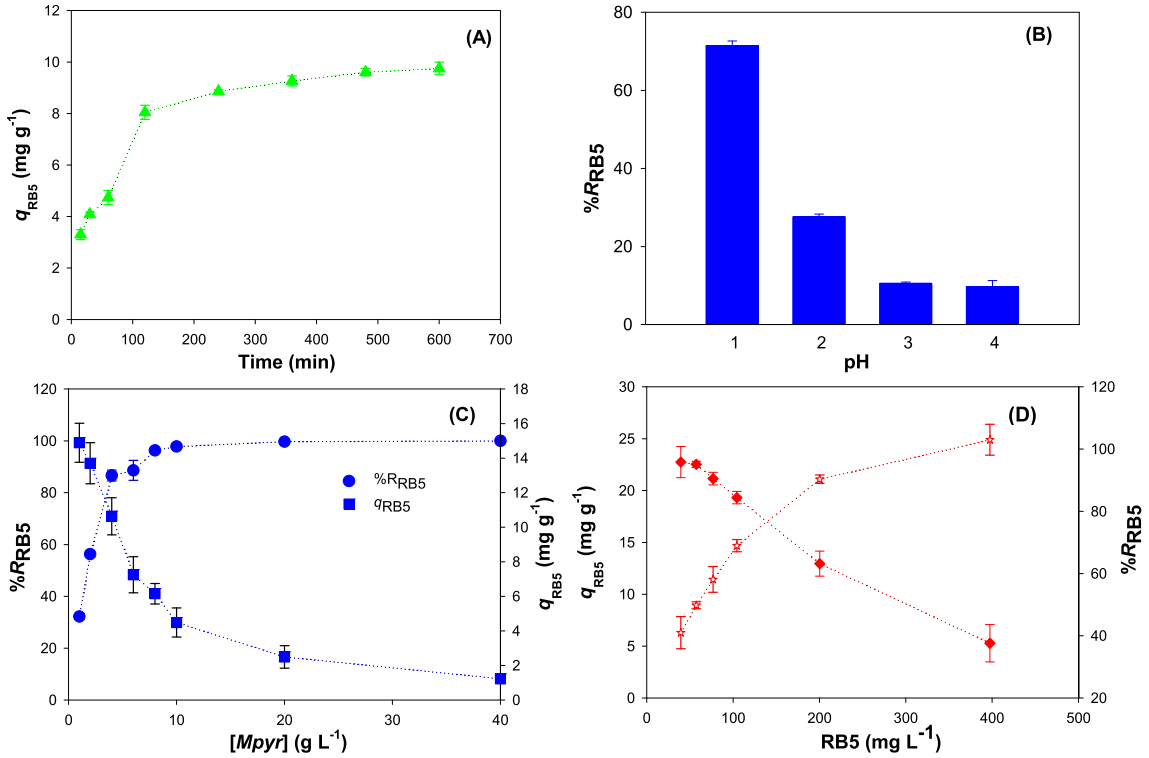

Fig. 2. Influence of operational parameters on RB5 biosorption onto *Mpyr*. A) Effect of contact time; B) effect of pH; C) effect of biosorbent dose; D) effect of initial RB5 concentration. Conditions: unless indicated, [RB5] = 50 mg L^{-1}, [*Mpyr*] = 6.0 g L^{-1}, pH 1, CT = 6 h, stirring = 180 rpm, V = 100 mL, T = 30 °C.

the adsorption capacity (q) increased from 6.3 mg g^{-1} (96%) to 25.0 mg g^{-1} (38%) with increasing initial RB5 concentrations (pH 1, 6 h CT). These results can be explained because at the lowest initial dye concentrations, all dye molecules can interact with the binding sites on the biomass surface, leading to high sorption rates, while at the highest concentrations, binding sites on the biomass surface are fully and rapidly saturated, and no further biosorption takes place (Iscen et al., 2007).

According to these results, the optimal conditions for RB5 removal with *Mpyr* were settled with 6 g L^{-1} of *Mpyr*, pH 1 for 6 h CT.

3.2. Treatment of RB5 with N25 in batch

Experiments with RB5 (100 mg L^{-1}) using 0.5 g L^{-1} N25 at different initial pH values (1–9) were performed to establish initially the optimal CT. Fig. S1 (Appendix A, section S2) shows that 30 min were enough to achieve the maximum removal, with almost no changes at longer contact times. Fig. 3A resumes the %R_{RB5} achieved with different N25 amounts (0.05–0.5 g L^{-1}) at pH from 1 to 9 after 30 min in contact with [RB5]$_0$ = 100 mg L^{-1}. Fig. 3B indicates the amount of total Fe in solution at different pH values using [N25]$_0$ = 0.5 g L^{-1}.

The highest RB5 removal percentage (96%) was obtained with the highest amount of N25 (0.5 g L^{-1}) at pH 3. This trend with the nZVI dosage is similar to that obtained by Satapanajaru et al. (2011), but our result is slightly better, as the authors obtained a similar removal efficiency under the same experimental conditions but after 3 h CT; the difference can be attributable to the higher surface area (i.e., higher number of active sites) of the nZVI used in the present work (i.e., 14 m^2 g^{-1} (Satapanajaru et al., 2011) vs. 20–25 m^2 g^{-1} (Nanoiron, 2017)).

The higher removal at acid pH values, also observed by Satapanajaru et al. (2011), can be explained by the fact that, at pH < 8, nZVI are positively charged (Li et al., 2006; Sun, 2006), while RB5 is negatively charged (Guthrie, 1978), allowing a facile interaction of the dye with the material and its further reduction. Additionally, low pH values also favor the undesired corrosion of the nanoparticles and may remove the passivating layers from the nZVI core, the material becoming free to react with the azo bond of the dye molecules, and releasing Fe to the solution. Fig. 3B shows that the highest amount of Fe in solution after 30 min CT and 0.5 g L^{-1} nZVI is observed at pH 1. At pH 5–9, no iron was found in solution. Although at pH 3 [Fe_{total}] after 30 min is around 90 mg L^{-1}, a value much higher than the maximum limits allowed by the Argentine Agency ACUMAR (2 mg L^{-1} and 10 mg L^{-1} for discharge of dissolved iron to surface water and sewer water bodies, respectively) (ACUMAR, 2017), this initial pH was selected as the best removal condition, due to the high removal efficiency achieved. It can be proposed that iron can be easily eliminated at the end of the experiment by adding an alkaline solution to induce iron precipitation.

Summarizing, the optimal conditions for RB5 removal with N25 were 0.5 g L^{-1} of nZVI, pH 3, for 30 min CT.

3.3. RB5 removal by Mpyr and N25 in series

Fig. 4 shows the removal efficiency of RB5 treated at different concentrations (100–400 mg L^{-1}) with *Mpyr* (6 g L^{-1}) at pH 1 for 6 h followed by treatment with nZVI (0.5 g L^{-1}) at pH 3 for 30 min, in the two possible sequential combinations, *Mpyr*/N25 (Fig. 4A) and N25/*Mpyr* (Fig. 4B).

Fig. 4A shows that the initial treatment with *Mpyr* resulted in removal percentages of 84, 71, and 45% for the three [RB5]$_0$, respectively, under the optimal conditions determined for *Mpyr*, indicating that the removal is more difficult as the [RB5] increases.

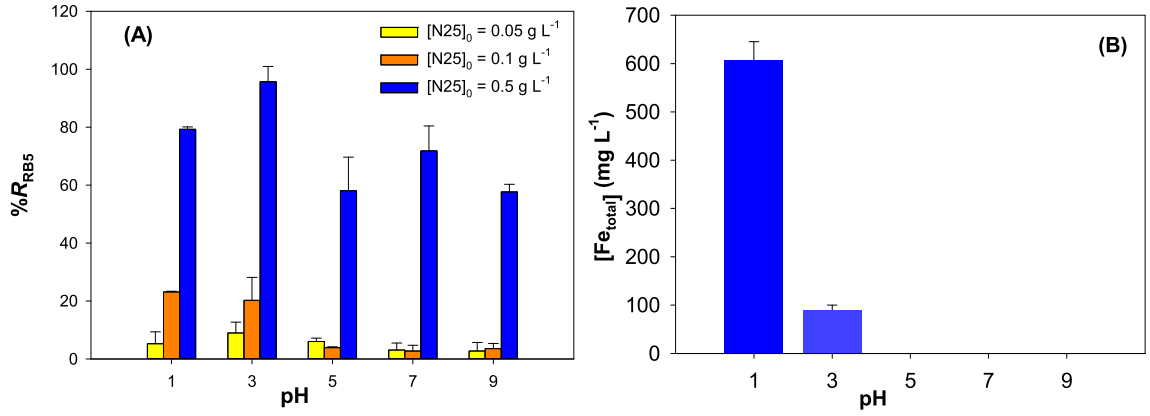

Fig. 3. (A) $\%R_{RB5}$ vs. initial pH and N25 load; (B) $[Fe_{total}]$ vs. initial pH using $[N25]_0 = 0.5$ g L^{-1}. Conditions: $[RB5]_0 = 100$ mg L^{-1}, CT = 30 min, stirring = 215 rpm.

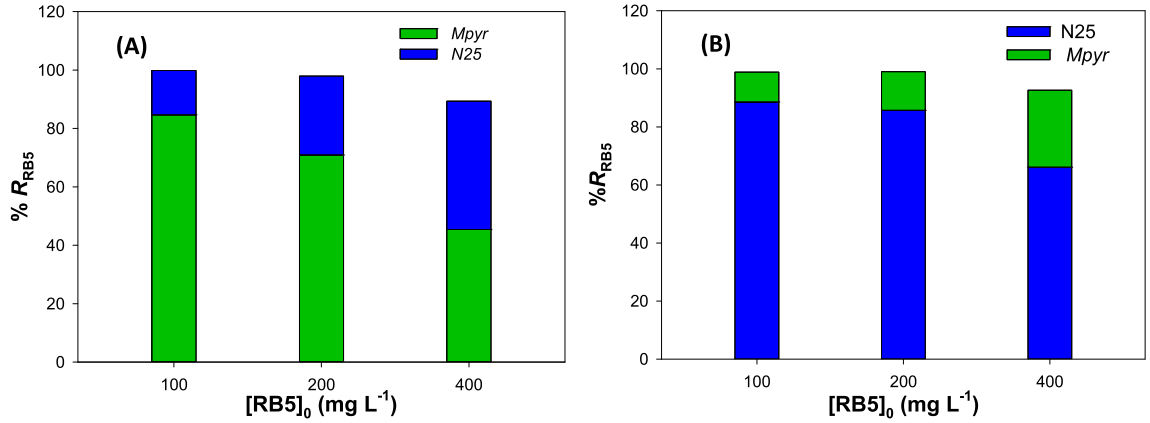

Fig. 4. $\%R_{RB5}$ for $[RB5]_0 = 100–400$ mg L^{-1} treated by in series experiments: (A) *Mpyr*/N25 and (B) nZVI/*Mpyr*. Conditions: [*Mpyr*] = 6 g L^{-1} (pH 1, CT = 6 h), [nZVI] = 0.5 g L^{-1} (pH 3, CT = 30 min, stirring = 215 rpm).

The removal increased after further treatment at the optimal conditions with N25, reaching high removal percentages (100, 98 and 89%, respectively). On the other hand, the use of N25 as the first step resulted in 89, 86 and 66% removal for the different concentrations, with an increase to 99, 99 and 92% with the further *Mpyr* treatment (Fig. 4B). Both treatments led to the almost complete color removal in the studied concentration range, with a higher removal efficiency than those obtained in the individual treatments after 6.5 h (i.e., sum of the CTs of the sequential treatments).

Results of TOC changes during the *Mpyr*/N25 and N25/*Mpyr* treatments and $[Fe_{total}]$ at the end of the experiments are displayed in Fig. 5.

The partial dissolution of alginate and other polysaccharides present in the surface of the *Mpyr* (Plaza et al., 2012b; Plaza Cazón et al., 2014) explains the increase of [TOC] after the treatment with *Mpyr* (Fig. 5A). The subsequent treatment with N25 removes 25–30% of the organic load present at this point. The final TOC values are higher than the limit imposed by ACUMAR for surface body water in terms of COD ($\leq$125 mg L^{-1}) but lower than the limit for sewer discharge water ($\leq$700 mg L^{-1}, ACUMAR, 2017) (see Appendix A, section S3). The TOC decrease after the *Mpyr*/N25 treatment is most likely due to adsorption of the organics released to solution by the *Mpyr* treatment onto the surface of the iron nanoparticles. Thus, the active sites of N25 become partially blocked reducing the removal capacity of the nanoparticles. Going back to Fig. 4, it can be seen that the individual treatment of $[RB5]_0 = 400$ mg L^{-1} at pH 3 with N25 gives a 66% (Fig. 4B) removal of the dye and reaches only a 45% removal after the use of *Mpyr* alone (Fig. 4A).

For the *Mpyr*/N25 sequence, final $[Fe_{total}]$ of 56.2, 68.1 and 76.2 mg L^{-1} (explained by the increase of the amount of RB5 removed, see blue bars in Fig. 4A) were obtained for $[RB5]_0 = 100$, 200 and 400 mg L^{-1}, respectively (Fig. 5B); these final concentration values are still higher than the limits imposed by ACUMAR, 2 and 10 mg L^{-1} for sewer and surface water, respectively (ACUMAR, 2017).

In Fig. 5C, corresponding to the TOC changes during N25/*Mpyr* treatment, direct reaction of RB5 with N25 results in a minor decline of the initial TOC value (due probably to adsorption by the nanoparticles), followed by a noticeable increase after the *Mpyr* treatment; TOC levels after the treatment with *Mpyr* as exclusive removal agent are 105, 127 and 175 mg L^{-1} (Fig. 5A) against 280, 244 and 251 mg L^{-1} after N25/*Mpyr* treatment for $[RB5]_0 = 100$, 200 and 400 mg L^{-1} (Fig. 5C). The final TOC values are higher than those obtained with the *Mpyr*/N25 sequence (cf. Fig. 5A and C) but still under the ACUMAR limit for sewer water (ACUMAR, 2017).

Fig. 5D indicates that, as expected, after the N25 treatment, $[Fe_{total}]$ increases by partial dissolution of the nanoparticles, but part of the initially dissolved iron is effectively trapped by the further biomass treatment, leaving, at most, $[Fe_{total}] = 16.13$ mg L^{-1} for $[RB5]_0 = 400$ mg L^{-1}. As stated by Miller et al. (2016), iron can bind to the surface of *Mpyr* through alginate carboxylate groups present in the cell wall of the algae, decreasing the amount of Fe in solution by this treatment.

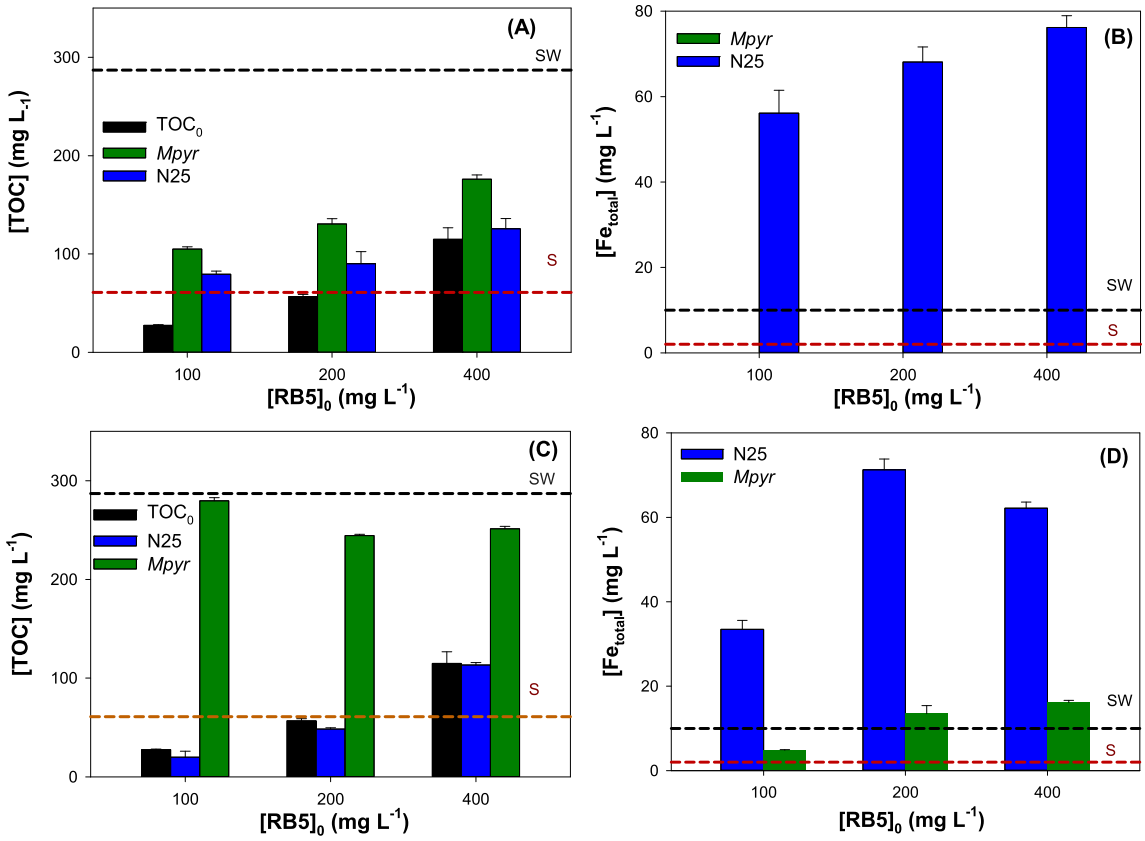

Fig. 5. (A) Changes in [TOC] and (B) [Fe_{total}] after RB5 removal ([RB5]$_0$ = 100–400 mg L^{-1}) with *Mpyr*/N25; (C) changes in [TOC] and (D) [Fe_{total}] after RB5 removal ([RB5]$_0$ = 100–400 mg L^{-1}) with N25/*Mpyr*. Conditions of Fig. 4. Black and red dotted lines correspond to sewer (SW) and surface water (S) limits established by ACUMAR (2017). (For interpretation of the references to colour in this figure legend, the reader is referred to the web version of this article.)

HPLC experiments were performed after each stage of the in series treatments. The chromatogram after the treatment of 100 mg L^{-1} of RB5 with *Mpyr*/N25 is shown in Fig. S2A (Appendix A, section S4), where sulfanilic acid was identified by comparison against a standard. In contrast, after the N25/*Mpyr* treatment, no sulfanilic acid could be detected (Fig. S2B), suggesting that this compound is efficiently adsorbed by *Mpyr*. Although Satapanajaru et al. (2011) reported the formation of 1-sulfonic-2-(4-amino-benzenesulfonyl) ethanol after the treatment of RB5 with nZVI, no evidence of this product was found in our work. It can be proposed that, under our conditions, the reductive desulfonylation of the above-mentioned intermediate takes place during the treatment with nZVI. If some other compounds are formed in the system, they could not be identified in our work. This indicates that N25/*Mpyr* is the most adequate combination for RB5 treatment, as *Mpyr* can successfully adsorb the intermediates generated during N25.

3.4. Simultaneous use of N25 and Mpyr

Experiments of RB5 removal with both materials, N25 and *Mpyr*, simultaneously present in the reaction system (*Mpyr* + N25) were performed and the results are shown in Fig. 6. It has been said above that the individual treatments required an optimum CT of 6 h and 30 min for *Mpyr* and N25, respectively. Thus, the optimum CT for the simultaneous treatment was first explored at pH 1 and 3, measuring the TOC changes and [Fe_{total}] at the end of the experiment.

Fig. 6A shows the temporal evolution of 100 mg L^{-1} RB5 removal at pH 1 and pH 3 using simultaneously 6 g L^{-1} *Mpyr* and 0.5 g L^{-1} N25. It can be seen that, at both pH values, no further RB5 removal after 60 min CT takes place. This is a clear advantage compared with the strategy of the sequential experiments, where the minimum CT was around 6.5 h, i.e., the sum of the time span of each separated process.

Fig. 6B shows the global efficiency for RB5 removal after 60 min CT. A smaller global removal efficiency was achieved in the combination *Mpyr* + N25 with respect to the in series experiments (% R_{RB5} > 89% compared with 60–80% for the simultaneous configuration (*Mpyr* + N25), cf. Figs. 4 and 6B). On the other hand, it is worth to remark that the treatment at pH 1 maintains its performance at all the RB5 concentrations, but lower efficiencies were obtained at pH 3 as [RB5] increased, in line with the blocking of N25 active sites by *Mpyr* indicated above.

Fig. 6C and D show the remaining TOC and [Fe_{total}] after each combined treatment. At pH 3, the final [Fe_{total}] decreases due to the lower extent of corrosion of nZVI at the less acid pH, but higher TOC levels are present at the end of the experiments. These results are consistent with those obtained in the previous sections and represent a drawback in the overall performance of the removal method. However, the simultaneous combination of N25 and *Mpyr* represents an outstanding decrease in the CT needed for the process, i.e., from 6.5 h to 1 h.

3.5. Packed columns for RB5 removal

N25 was supported on *Mpyr* by wet impregnation under N_2 atmosphere at room temperature by a very simple procedure, leading to the N25@*Mpyr* material. According to Miller et al. (2016),

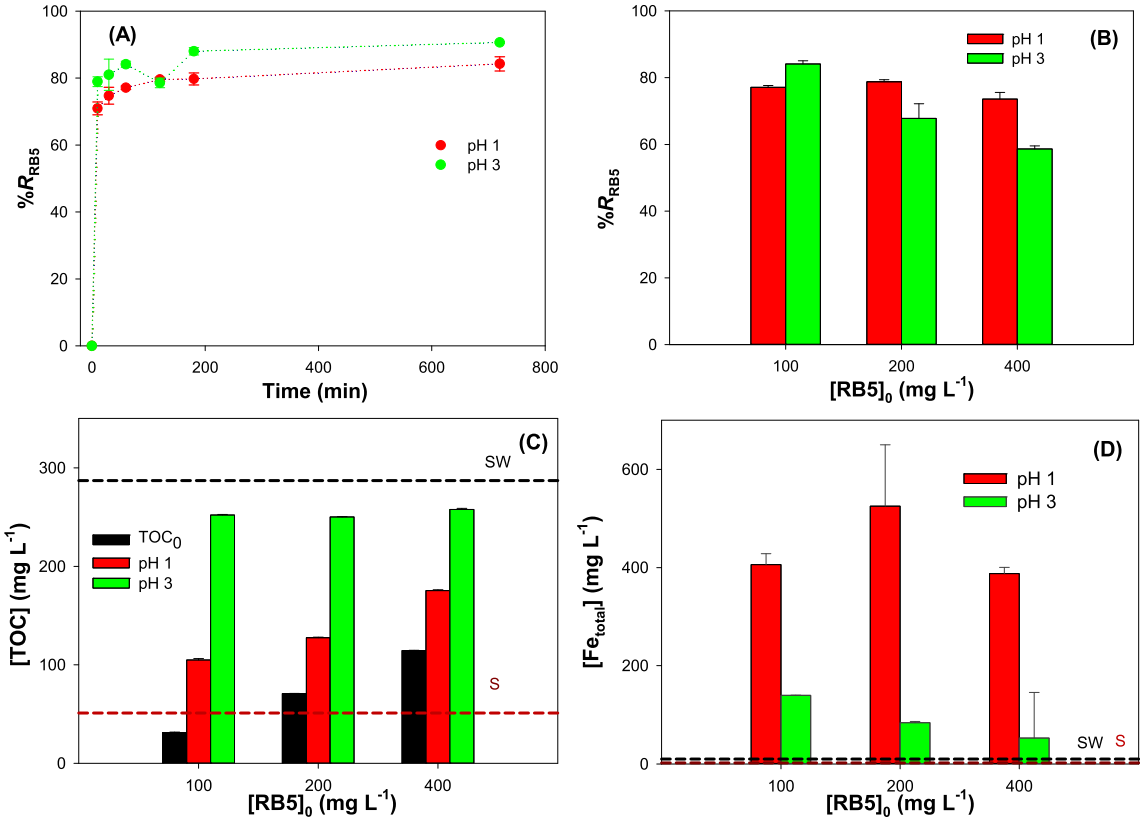

Fig. 6. Influence of pH in the removal of RB5 using the combination of N25 and *Mpyr* (*Mpyr* + N25) in: (A) CT, [RB5] = 100 mg L^{-1}; (B) removal efficiency at different [RB5]; (C) TOC changes at different [RB5]; (D) [Fe_{total}] at the end of experiments with different [RB5]. Conditions: unless indicated, [*Mpyr*] = 6 g L^{-1}, [N25] = 0.5 g L^{-1}, CT = 60 min, stirring = 215 rpm. Black and red dotted lines correspond to sewer (SW) and surface water (S) limits established by ACUMAR (2017). (For interpretation of the references to colour in this figure legend, the reader is referred to the web version of this article.)

carboxylate groups contained in the alginate present at the surface of *Mpyr* play a key role for the iron binding; particularly, Fe(III) has been used as crosslinking agent in the polymerization of alginate because of its high affinity towards polysaccharides (Giammanco et al., 2015). Therefore, it was found pertinent to test the possibility that surface bonded Fe(III) in the iron oxide outer layer of N25 could act as an anchoring point to immobilize the nanoparticles. In fact, SEM-EDS analysis performed on N25@*Mpyr* showed that the iron nanoparticles have been effectively immobilized on the surface of *Mpyr* (Fig. 7).

Fig. 7A shows a uniformly wrinkled surface corresponding to *Mpyr*. Fig. 7B shows that nZVI can be retained on the surface of the *Mpyr* after the immobilization procedure. The center of the image is dominated by a brighter agglomerate of nZVI and smaller bright spots corresponding to smaller agglomerates or individual nanoparticles distributed alongside the *Mpyr* surface. Fig. 7C displays the EDS spectra of *Mpyr* and N25@*Mpyr*, showing the presence of C, O, Ca and S as main elements in both samples and also Fe in the latter. The iron content in N25@*Mpyr* was approximately 27% (m/m) as estimated by EDS analysis. The XRD patterns corresponding to N25, *Mpyr* and N25@*Mpyr* before (b) and after (a) RB5 treatment are displayed in Fig. 7D. Fe^0 and magnetite (Fe_3O_4) or maghemite (γ-Fe_2O_3) are the main phases of iron present at the surface of N25@*Mpyr* before RB5 treatment, indicating that during the immobilization, part of the Fe^0 originally present is partially oxidized. Additionally, the pattern after RB5 treatment with N25@*Mpyr* shows increased signals of Fe^0 oxidation products (magnetite, maghemite and possibly lepidocrocite), as suggested by Pullin et al. (2017).

The material obtained in this way was used in column experiments for RB5 removal ($[RB5]_0$ = 100 mg L^{-1}, pH 3). The results are displayed in Fig. 8.

As Fig. 8 shows, the column reaches a sustained removal efficiency of ca. 70% up to 1170 pore volumes (175 mL), which then decreases until recovering the upstream RB5 concentration after 4200 pore volumes (630 mL). The use of bare *Mpyr* (inset of Fig. 8) leads to 20% removal for only 470 pore volumes. Satapanajaru et al. (2011) prepared a column filled with nZVI mixed with sand, and reported a discoloration efficiency of 80% up to 3800 mL of $[RB5]_0$ = 100 mg L^{-1} (pH 5). Despite a direct comparison is difficult as the pH of the RB5 solution was different and the authors do not show the column efficiency in terms of pore volumes, the performance of the N25@*Mpyr* column used in this work seems to be better. They reported to use a 400 times higher column volume, obtaining just a 22 times (i.e., 3800 mL/175 mL) higher breakthrough volume.

TOC and [Fe_{total}] were also monitored in the column experiment with N25@*Mpyr*, and the results are summarized in Figs. S3 and S4 (Appendix A, section S5). TOC increases by partial dissolution of *Mpyr* cell wall components up to ca. 100 mg L^{-1} at 280 pore volumes. From that point, the TOC concentration consistently decreases to ca. 30 mg L^{-1} at around 2300 pore volumes. Considering that the initial TOC value for 100 mg L^{-1} of RB5 is 31.5 mg L^{-1}, these results imply that the loss of color is most likely due to reduction of RB5 by N25, with no or little adsorption of the intermediates onto the *Mpyr* surface.

The [Fe_{total}] profile over pore volume had a more erratic behavior, reflected by the large error bars, but the average slightly

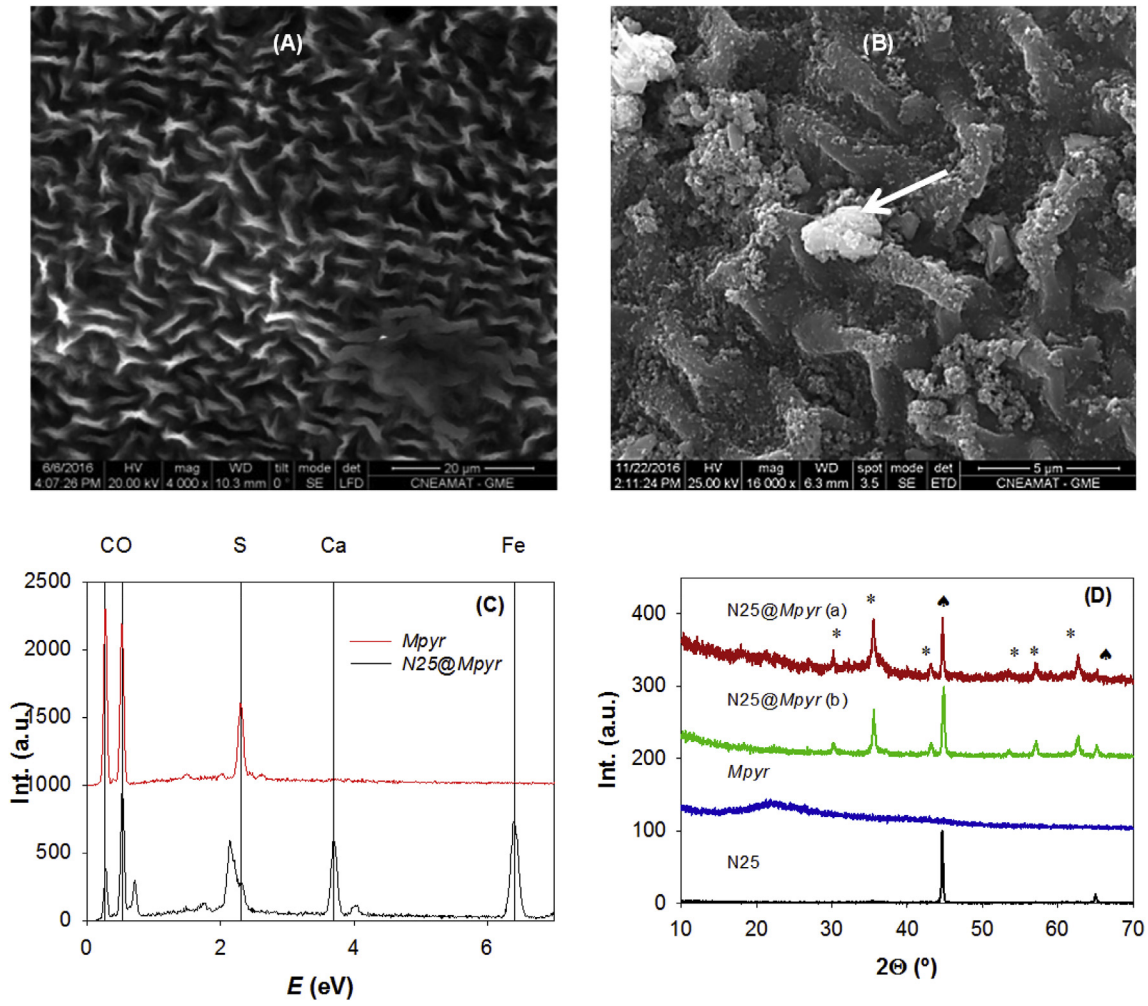

Fig. 7. SEM images of (A) *Mpyr* and (B) and N25@*Mpyr*; (C) EDS spectra of both samples and (D) XRD patterns for N25, *Mpyr* and N25@*Mpyr* before (b) and after (a) RB5 treatment. The arrow in (B) indicates an iron nanoparticle agglomerate. In (D), * and ♠ represent the XRD peaks for α-Fe and magnetite or maghemite.

decreases after a high initial dissolution of Fe. The high initial dissolution is also indicative of the color removal by chemical reduction of the azo bond in the dye and the loss of efficiency over time consistently with the appearance of oxidized phases of iron (Fig. 7D for N25@*Mpyr* after RB5 treatment). The area above the breakthrough curve in Fig. 8 was calculated by integration between 0 and 630 mL, and a full capacity of 39.9 mg RB5/g of N25@*Mpyr* was obtained, which was higher than the capacity calculated for the removal of $[RB5]_0 = 100$ mg L^{-1} at pH 3 in batch with the simultaneous treatment (12.9 mg RB5/g of (N25 + *Mpyr*), see Fig. 6B and Appendix A, section S6, Eq. S1). The difference can be explained by two factors. On one hand, the filling of the column has a higher concentration of iron: ca. 27% for in N25@*Mpyr* and only 7.7% for the N25 + *Mpyr*. On the other hand, the batch experiment under agitation continuously incorporates O_2 from the air, while the column setup restrains the dissolution of additional O_2 once the experiment begins, thus preserving the immobilized nZVI from additional corrosion.

4. Conclusions

The removal of RB5 can be successfully achieved by a combination of reduction with nZVI and/or adsorption on *Mpyr*. The removal efficiency of these materials showed a different dependence on pH: N25 reaches its maximum RB5 removal capacity at pH 3, while *Mpyr* efficiency decreases as the pH rises from 1. In series and simultaneous combination of these two processes were studied at both pH conditions, showing a high removal capacity ($\%R_{RB5} > 80\%$). However, both removal agents introduce species in the system at the selected pH conditions: N25 introduces Fe coming from its corrosion, and *Mpyr* releases polysaccharides that increase the TOC in solution.

It can be concluded that the in series processes have no clear advantage over the individual treatments as they do not prevent the release of organic species from *Mpyr* or iron from N25, with a long reaction time (6.5 h), resulting from the sum of both separated treatments. On the other hand, the simultaneous use of *Mpyr* and N25 led to a remarkable removal efficiency in only 1 h of treatment.

The column experiments with N25 adsorbed on *Mpyr* (N25@*Mpyr*) showed a higher removal capacity than the experiments in batch, and contribute with a novel approach to the combination of a biological and a physicochemical treatment for the removal of azo dyes in solution.

Although conventionally synthesized iron nanomaterials may pose toxicity when used at high doses, no significant phytotoxic effects have been found on some plant species when exposed to high nZVI concentrations, in contrast with TiO_2 nanoparticles (Goswami et al., 2017). Toxicity can be further reduced by the

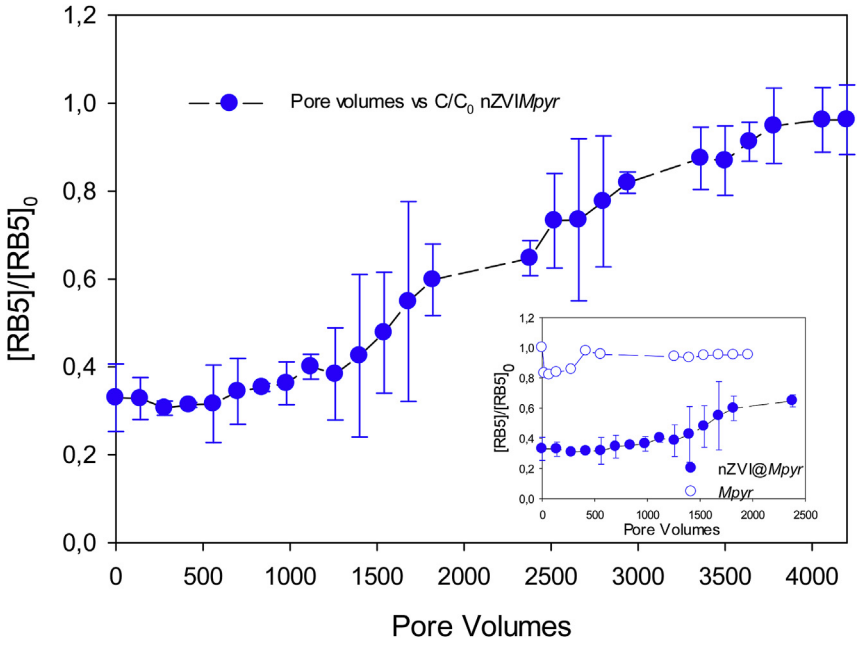

Fig. 8. Breakthrough curve for N25@*Mpyr* with $[RB5]_0$ = 100 mg L^{-1} at pH 3. Inset: breakthrough curve for *Mpyr* and N25@*Mpyr* up to 2500 pore volumes. Conditions: $[RB5]_0$ = 100 mg L^{-1}, pH 3, flow = 0.35 mL min^{-1}, pore volume = 0.15 mL.

addition of capping agents, enhancing reactivity (Das et al., 2016). This indicates that toxicity can be expected not to increase by the use of the materials proposed in this work. Toxicity studies will be attempted in the future.

Acknowledgements

This work was partially supported by Agencia Nacional de Promoción Científica y Tecnológica of Argentina, PICT-2011-0463, PICT-2015-0208 and PICT-2015-0463 grants and by the PIO CONICET-YPF 2014–2015 13320130100022CO grant.

Appendix A. Supplementary data

Supplementary data related to this article can be found at https://doi.org/10.1016/j.jenvman.2017.11.002.

References

ACUMAR, (2017) http://www.acumar.gov.ar/content/documents/2/6172.pdf (accessed on 26/01/2017).
Boraso, A., Zaixo, J.M., 2012. Algas marinas bentónicas. In: Boltovskoy, D. (Ed.), Atlas de Sensibilidad Ambiental de la Costa y el Mar Argentino. http://seaweedafrica.org/pdf/562DF4FA1149b1C475TSK191032E/48288.pdf. (Accessed 18 October 2012).
Chatterjee, S., Lim, S.-R., Woo, S.H., 2010. Removal of Reactive Black 5 by zero-valent iron modified with various surfactants. Chem. Eng. J. 160, 27–32.
Chompuchan, C., Satapanajaru, T., Suntornchot, P., Pengthamkeerati, P., 2009. Decolorization of reactive black 5 and reactive red 198 using nanoscale zerovalent iron. World Acad. Sci. 3, 1–11. Engineering and Technology International Journal of Chemical, Molecular, Nuclear, Materials and Metallurgical Engineering (WASET).
Crini, G., 2006. Non-conventional low-cost adsorbents for dye removal: a review. Bioresour. Technol. 97, 1061–1085.
Das, P., Sarmah, K., Hussain, N., Pratihar, S., Das, S., Bhattacharyya, P., Patil, S.A., Kim, H.-S., Khazi, M.I.A., Bhattacharyya, S.S., 2016. Novel synthesis of an iron oxalate capped iron oxide nanomaterial: a unique soil conditioner and slow release eco-friendly source of iron sustenance in plants. RSC Adv. 6, 103012–103025.
El-Zawahry, M.M., Abdelghaffar, F., Abdelghaffar Rehab, A., Hassabo, A.G., 2016. Equilibrium and kinetic models on the adsorption of Reactive Black 5 from aqueous solution using *Eichhornia crassipes*/chitosan composite. Carbohydr. Polym. 136, 507–515.
Fakhry Eman, M., 2013. *Padina pavonica* for the removal of dye from polluted water. Am. J. Plant Sci. 4, 1983–1989.
Fan, J., Guo, Y., Wang, J., Fan, M., 2009. Rapid decolorization of azo dye methyl orange in aqueous solution by nanoscale zerovalent iron particles. J. Hazard Mater. 166, 904–910.
Giammanco, G.E., Sosnofsky, C.T., Ostrowski, A.D., 2015. Light-responsive Iron(III)-polysaccharide coordination hydrogels for controlled delivery. ACS Appl. Mater. Inter 7, 3068–3076.
Goswami, L., Kim, K.-H., Deep, A., Das, P., Bhattacharya, S.S., Kumar, S., Adelodun, A.A., 2017. Engineered nano particles: nature, behavior, and effect on the environment. J. Environ. Manag. 196, 297–315.
Guthrie, J.P., 1978. Hydrolysis of esters of oxy acids: pKa values for strong acids; Brønsted relationship for attack of water at methyl; free energies of hydrolysis of esters of oxy acids; and a linear relationship between free energy of hydrolysis and pKa holding over a range of 20 pK units. Can. J. Chem. 56, 2342–2354.
Huang, J., Liu, D., Lu, J., Wang, H., Wei, X., Liu, J., 2016. Biosorption of reactive black 5 by modified *Aspergillus versicolor* biomass: kinetics, capacity and mechanism studies. Colloid Surf. A 492, 242–248.
Iscen, C.F., Kiran, I., Ilhan, S., 2007. Biosorption of reactive black 5 dye by *Penicillium restrictum*: the kinetic study. J. Hazard Mater. 143, 335–340.
Li, D.W., Elliott, W., Zhang, 2006. Zero-valent iron nanoparticles for abatement of environmental pollutants: materials and engineering aspects. Crit. Rev. Solid State Mater. Sci. 31, 111–122.
Low, K.S., Lee, C.K., Toh Pertanika, B.L., 1994. Binding of basic dyes by the algae *Chara aspera*. J. Sci. Technol. 2, 85–92.
Matheickal, J.T., Qiming, Y., 1999. Biosorption of lead(II) and copper(II) from aqueous solutions by pre-treated biomass of Australian marine algae. Bioresour. Technol. 69, 3094–3099.
Miller, E.P., Auerbach, H., Schü, V., Tymon, T., Carrano, C.J., 2016. Surface binding, localization and storage of iron in the giant kelp *Macrocystis pyrifera*. Metallomics 8, 379–462.
Montesinos, V.N., Quici, N., Beatriz Halac, E., Leyva, A.G., Custo, G., Bengio, S., Zampieri, G., Litter, M.I., 2014. Chem. Eng. J. 244, 569–575.
Nanoiron, 2017 http://www.nanoiron.cz/en/nanofer-25 (accessed on 05/07/2017).
Plaza Cazón, J., Viera, M., Donati, E., Guibal, E., 2013a. Zinc and cadmium removal by biosorption on *Undaria pinnatifida* in batch and continuous processes. J. Environ. Manag. 129, 423–434.
Plaza Cazón, J., Viera, M., Donati, E., 2013b. Dynamic Cr(III) uptake by *Macrocystis pyrifera* and *Undaria pinnatifida* biomasses. Electron. J. Biotechnol. 16, 1–11.
Plaza Cazón, J., Viera, M., Sala, S., Donati, E., 2014. Biochemical characterization of *Macrocystis pyrifera* (Linnaeus) C. Agardhand *Undaria pinnatifida* (Harvey) Suringar (Phaeophyceae) in relation to their potentiality as biosorbents. Phycologia 53, 100–108.
Plaza, J., Benitez, L., Viera, M., Donati, E., 2012a. Equilibrium and kinetic study of the biosorption of chromium (III) by two brown algae: *Macrocystis pyrifera* and *Undaria pinnatifida*. Eng. Life Sci. 12, 95–103.
Plaza, J., Bernardelli, C., Viera, M., Donati, E., Guibal, E., 2012b. Zinc and cadmium biosorption by untreated and calcium-treated *Macrocystis pyrifera* in a batch

system. Bioresour. Technol. 116, 195–203.
Plaza, J., Viera, M., Donati, E., Guibal, E., 2011. Biosorption of mercury by *Macrocystis pyrifera* and *Undaria pinnatifida*: influence of zinc, cadmium and nickel. J. Environ. Sci. 23, 1778–1786.
Pullin, H., Springell, R., Parry, S., Scott, T., 2017. The effect of aqueous corrosion on the structure and reactivity of zero-valent iron nanoparticles. Chem. Eng. J. 308, 568–577.
Raman, C.D., Kanmani, S., 2016. Textile dye degradation using nano zero valent iron: a review. J. Environ. Manag. 177, 341–355.
Rubín, E., Rodríguez, P., Herrero, R., Sastre de Vicente, M.E., 2010. Adsorption of methylene blue on chemically modified algal biomass: equilibrium, dynamic, and surface data. J. Chem. Eng. Data 55, 5707–5714.
Shang, J., Zong, M., Yu, Y., Kong, X., Du, Q., Liao, Q., 2017. Removal of chromium(VI) from water using nanoscale zerovalent iron particles supported on herb-residue biochars. J. Environ. Manag. 197, 331–337.
Satapanajaru, T., Chompuchan, C., Suntornchot, P., Pengthamkeerati, P., 2011. Decolorization of Reactive Black 5 and Reactive Red 198 using nano scale zerovalent iron. Desalination 266, 218–230.
Sun, Y.-P., 2006. Characterization of zero-valent iron nanoparticles. Adv. Colloid Interface Sci. 120, 47–56.
Sun, Y., Li, J., Huang, T., Guan, X., 2016. The influences of iron characteristics, operating conditions and solution chemistry on contaminants removal by zero-valent iron: a review. Water Res. 100, 277–295.
Vijayaraghavan, K., Yun, Y.-S., 2008. Biosorption of C.I. Reactive Black 5 from aqueous solution using acid-treated biomass of brown seaweed *Laminaria* sp. Dyes Pigments 76, 726–732.
Yagub, M.T., Sen, T.K., Afroza, S., Ang, H.M., 2014. Dye and its removal from aqueous solution by adsorption: a review. Adv. Colloid Interface Sci. 209, 172–184.